AL03 - A Modernized ANSYS-Based Finite Element Model for the Thermal-Electrical Design of Aluminum Reduction Cells

Daniel Richard[1], André Felipe Schneider[2], Marc Dupuis[3] and Stephan Broek[4]
1.Associate – Center of Excellence for Aluminum, Hatch Ltd., Saguenay, Canada
2. Numerical Analysis Specialist – Center of Excellence for Aluminum, Hatch Ltd., Montréal, Canada
3. Consultant, GeniSIM, Inc., Saguenay, Canada
4. Associate – Center of Excellence for Aluminum, Hatch Ltd., Mississauga, Canada
Corresponding author: daniel.richard@hatch.com

Abstract

Heat balance and magnetohydrodynamics are critical to the design of an aluminum reduction cell since they largely determine its operational window. Furthermore, an inadequate lining design generally leads to degraded cell performance and premature failures. The first task in lining design is to determine the position of the frozen ledge and the cell superheat for a range of operational parameters.

Although several different modeling approaches and computational domains have been proposed to solve the Stefan problem, a widely accepted methodology, first proposed by Dupuis [1], is based on the iterative repositioning of the ledge front in a thermoelectrical (TE) Finite Element (FE) model. The algorithm involves successive displacements of the solidification front nodes based on the calculated temperature field until the entire ledge-to-liquids interface reaches the bath solidification temperature. The superheat is adjusted to minimize the difference between the cell internal heat generation and the integrated heat losses over the control volume. Originally, this approach was limited to two layers of first order elements across the ledge thickness moving horizontally and did not include the liquids.

This paper presents a generalization as well as improvements to the original methodology, enabling the prediction of the ledge profile using an arbitrary number of first or second order elements through the ledge thickness while including the metal pad and the bath. The proposed modeling framework has been implemented in ANSYS using the ANSYS Parametric Design Language (APDL) scripting language and designed to minimize the computational cost of moving the ledge. Another benefit is that the generic core macros developed also efficiently handle the ledge front displacement in any orientation. Current technology ANSYS elements are used, in such a manner that high-performance computing solvers can be leveraged.

The robustness of this improved methodology is illustrated in this article by comparing the results obtained for a fictitious 300 kA cell technology against those computed by the standard approach.

Keywords: Aluminum reduction cells, heat balance, moving ledge profile, finite element analysis.

1. Introduction

Hatch has long been involved in the assessment of aluminium reduction technologies for greenfield and brownfield smelter projects and has recently been mandated to evaluate designs for a brownfield retrofit project, and specifically to perform heat balance calculations. Numerical modeling is considered the best tool to study the thermal-electrical behavior of the lining and the methodology is mature and widely accepted.

An essential part of the modelling effort is to predict the ledge profile, which can be quite challenging. Dupuis first developed a FORTRAN routine to reposition the ledge of a cathode slice and solved the TE problem by means of a finite element analysis in the commercial software ANSYS. The approach was then implemented in the ANSYS interpreted scripting language APDL [1]. The model domain was progressively enlarged to include a full quarter cell [2] but did not include the liquid phases at this point. The electrical boundary conditions were applied to the immerged surface of the anodes and to the top surface of the cathode blocks as an electrical equipotential.

Dupuis introduced a full cell slice (*i.e.* including both anode and cathode segments) with combined convergence of cell superheat and the ledge profile in [3]. The liquid zone for the full quarter was later introduced in [4] thus allowing one to obtain a representative current distribution in the metal pad.

The same modeling approach to move the ledge continued to be employed by Dupuis from the mid-1980's up to his most recent work in 2019 [5]. During that period, the ANSYS software platform has evolved, such that some of the functionalities used by Dupuis became no longer entirely compatible with the most recent versions of said software package.

Furthermore, the Authors agree that some of the drawbacks of the original Dupuis approach are the following:

The construction of the geometry is from the bottom-up and requires experience with ANSYS APDL

The discretization of the domain is limited to linear elements

In particular, the discretization of the ledge thickness is limited to 2 elements

The ledge mesh is attached to the cathode surface, which is limiting for the construction of the corner geometry. It also limits the position of the ledge toe as it depends on the cathode block assembly topology

The processing time for moving ledge and update boundary conditions is substantial

The models are based on legacy ANSYS elements

- These elements do not support present-day Distributed Memory Parallel (DMP) processing, which substantially increases computational performance of large models
- Furthermore, thermal loads are, in some instances, applied directly to the faces of solid elements, which is no longer supported by some of the current-technology ones (e.g., SOLID231).

From all of the above, it became quite clear that the original Dupuis approach could be improved in order to obtain a modernized methodology that is fully compatible with ANSYS 2020 R1. This was accomplished by rewriting critical routines and restructuring the modeling workflow.

2. Modernized Approach Workflow

The new workflow is summarized in Figure 1.

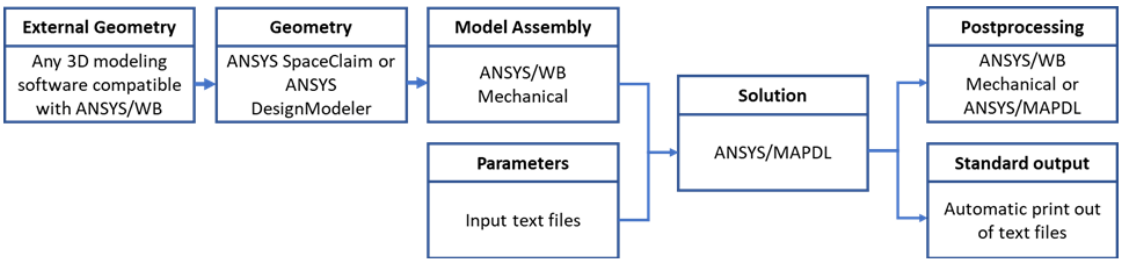

Figure 1. Modernized approach workflow.

2.1 External Geometry

Solid geometry of a cell can be developed in any software package compatible with the ANSYS geometry engines and imported for further processing. Examples of valid geometry formats include CATIA, Parasolid, STL, and STEP files.

2.2 Geometry Editing

The geometry that is tied to the model assembly is built with either ANSYS/SpaceClaim or ANSYS/Design Modeler. Within the context of the present work, the Authors used SpaceClaim to preprocess the geometry. External components can be imported and modified, while additional entities (e.g., the ledge) can be added directly in this module. Bodies are regrouped into parts that share a mesh and the interaction between different parts is handled by contact-target element pairs when building the finite element model itself.

2.3 Finite Element Model Assembly

The geometry is linked into ANSYS/Workbench (WB) Mechanical environment, where the finite element (FE) mesh is built and contact is established between parts that do not share a mesh. Named components are also defined in this environment.

The ANSYS/WB Mechanical environment is shown in Figure 2. The colors represent the different parts in the model that will share a FE mesh. Contact and target elements are used to transfer heat and electricity across non-matching meshes from the different parts, which facilitate the discretization of the domain.

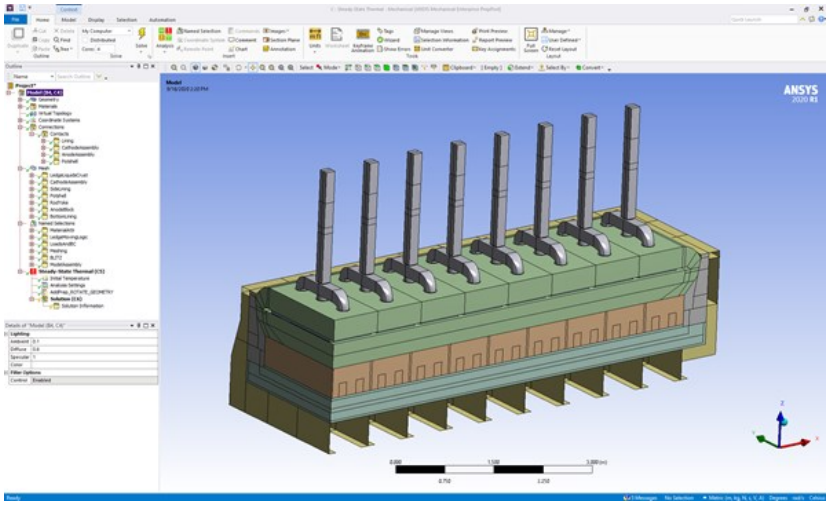

Figure 2. ANSYS/WB Mechanical environment with a quarter cell model.

Named selections (or, simply, components) are used in APDL routines to:
Assign materials properties
Assign element types and physics (e.g., thermal shell, thermal-electrical solid, etc.);
Define contact and target surfaces
Apply boundary conditions, like surface convection or prescribed voltages
Define the entities required for the ledge repositioning logic
Define the heat balance control volume
Define the reference location for reporting the anodic and cathodic voltage drops
Define the boundaries of the cell control volume at the anodic and cathodic panels

Define the bodies included in the finite element solution but that are outside of the cell control volume
Define the surfaces for the detailed heat losses output
Define model assemblies for different types of solution (e.g., half anode, quarter anode panel, cathode slice, full cell slice, quarter cathode panel and full cell quarter).

Examples of named selections can be found in Figure 3. A typical FE mesh is shown in Figure 4, with coloring corresponding to the element types.

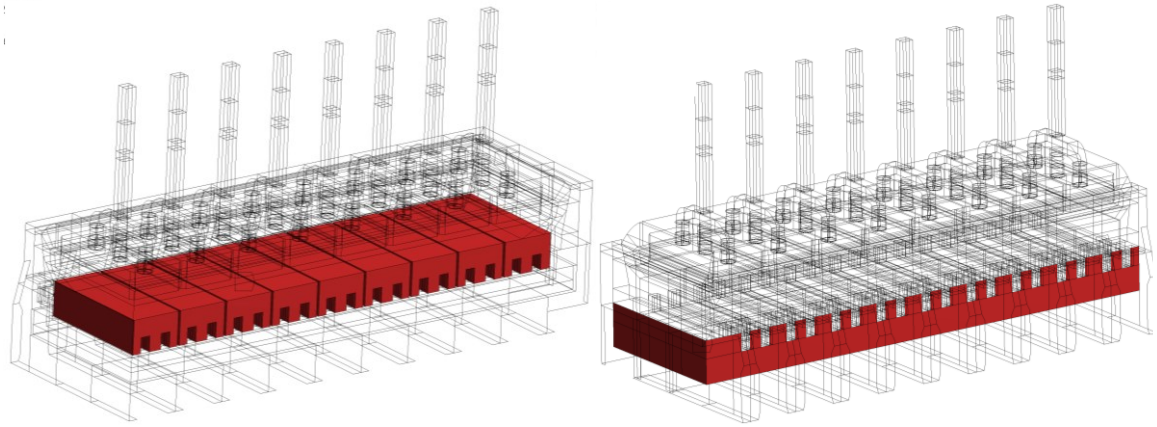

Figure 3. Example of named selections (or components). Left: component identifying the cathode blocks for the attribution of material properties. Right: named selection identifying the lower part of the pot shell for the definition of convection and radiation boundary conditions.

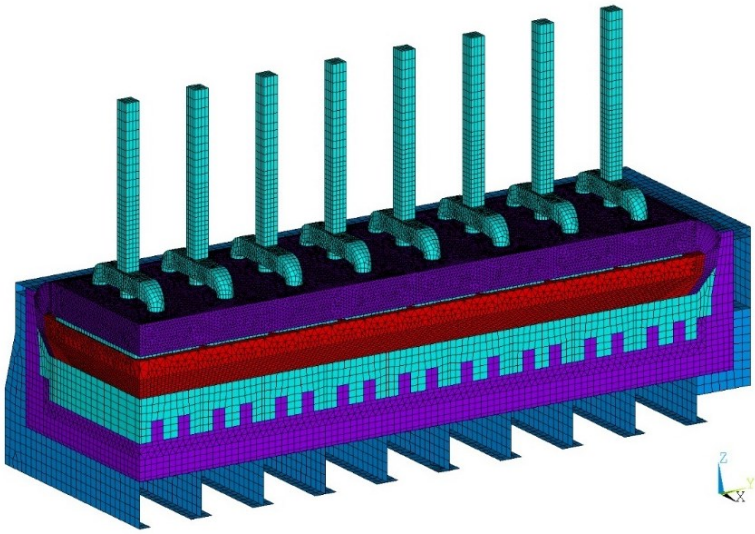

Figure 4. Initial FE linear mesh for a full quarter cell model.

It is important to highlight that, once the FE mesh is built, there is no need to return to any of the ANSYS/WB instances (either ANSYS/SpaceClaim, ANSYS/Design Modeler or ANSYS/WB Mechanical environments) while computing the solution as the prediction of both operating temperature and superheat as well as the repositioning of the ledge-liquids interface and the update of heat transfer boundary conditions are entirely handled by generic APDL macros, which require no User intervention (refer to section 2.5).

2.4 Parameters

Once the mesh is built and all the components are defined, the User needs to update the input text files required for the solution. Model parameters defined in text files will be read by ANSYS/APDL routines. These User input parameters are organized into four (4) main files:

General parameters file. This includes, for example, the cell amperage, the bath chemistry, the ambient temperature, the model domain and the type of solution.

Materials and physics file. This is where the material properties are assigned to named selections and the appropriate physics is selected.

Boundary conditions file. This is where convection and radiation heat transfer surface loads are defined by the User and assigned to components.

Heat losses output definition file. This file is used to list the named selections that will be used for the detailed heat losses standardized output.

2.5 Solution

Generic APDL macros are used to process the ANSYS Workbench database together with the four (4) input text files described above. This can be done either interactively within the ANSYS/WB Mechanical module, or separately as a batch solution running in the background. Note that the User does not need to edit any of the generic macros to perform an analysis.

The following steps occur during this phase:
Reading of the ANSYS Workbench database;
Reading of the general parameters;
Reselecting the appropriate model domain;
Creating and reading the material properties;
Assigning the material properties and the element types;
Creation of the required contact-target element pairs;
Creation of the auxiliary data structure for the ledge repositioning logic;
Creation of the heat transfer coefficients;
Application of the heat transfer loads and the electrical boundary conditions;
Reading of the surfaces for the heat losses detailed output;
Definition of the extrapolation factors required for the complete cell output heat losses corresponding to the model domain;
Application of the settings for the nonlinear thermal-electrical solution;
Solving the problem by following one (1) of three (3) possible routes, namely:

- Static solution for half anode and anode panel models (*i.e.*, thermal-electrical problem solved only once);
- Ledge convergence only for cathode slice and quarter cathode models at fixed superheat, or;
- Simultaneous superheat and ledge convergence for full cell slice and full cell quarter models.

2.6 Postprocessing

Postprocessing of results can either be programmed in APDL macros or done interactively in ANSYS. A typical temperature distribution is shown in Figure 5.

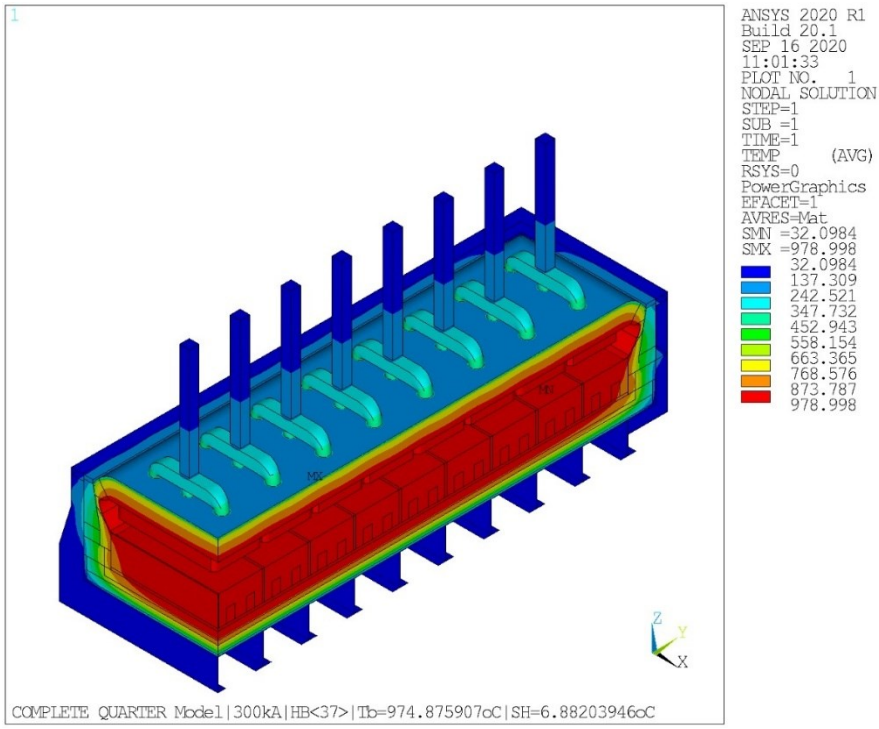

Figure 5. Full quarter cell temperature distribution (°C) at converged ledge and superheat.

2.7 Standard Output

Once the global problem has converged, a standard output text file is created that summarizes the results and details the heat losses on the previously defined surfaces. An example is shown in Figure 6 for the ledge convergence solution of a quarter cathode model (*i.e.*, no anode panel) using a quadratic FE mesh. Note that the detailed heat losses are reported for the model domain, which means that the User must multiply the heat flow by the appropriate scaling factor for the cell – in the particular case of a quarter cell model, by four (4).

```
=========================================================
      CATHODE QUARTER Model
      Solution type     Ledge convergence only
=========================================================
OPERATING CONDITIONS
---------------------------------------------------------
  Cell Current                [kA]  300.00
  Operating Temperature       [°C]  975.00
  Liquidus                    [°C]  968.00
  Superheat                   [°C]  7.00
  Ambient temperature         [°C]  20.00
=========================================================
HEAT IN
---------------------------------------------------------
  Bath to ledge               [kW]  83.29
  Metal to ledge              [kW]  173.78
  Metal to lining             [kW]  53.87
  Joule Heat in Cathode       [kW]  91.92
  Total Heat into Cathode     [kW]  402.87
  Cathode Voltage Drop        [mV]  295.09
=========================================================
GLOBAL HEAT LOST
```

```
-------------------------------------------------
  Cathodic Panel               [kW]  402.826818
-------------------------------------------------------------
DETAILED HEAT LOST OVER MODEL DOMAIN
-------------------------------------------------------------
    [W]          [W/m2]     [Component]
   7171.42     5242.27     CollBars
   3956.95     1373.25     CathodeFlexes
   1502.86     1097.98     Deckplate_In
  36662.16     6004.28     SW_AboveBars
   2930.94     2461.33     SW_BarLevel
   1435.80      561.74     SW_BelowBars
   1357.28       70.57     SW_CradlesFlange
  10802.30      336.71     SW_CradlesWeb
   7843.77     1086.40     SW_DeckPlate_Out
   6674.86      432.24     Shell_Floor
   1252.41      928.74     EW_BelowBox
   1928.73      675.70     EW_Box
    108.84      331.82     EW_CradlesFlange
    420.19      333.48     EW_CradlesWeb
   2092.54      911.78     EW_Deckplate_Out
   9900.20     5292.81     EW_InsideBox
   4665.44    31003.70     Heat leaving cathodic CV
      0.00                 Joule Heat outside cathodic CV
=============================================================
ERROR CALCULATION
-------------------------------------------------------------
  Ledge converged?                                 [-]  Yes
  Ledge Max (infinite norm) Temperature error*     [°C] 8.88
  Ledge RMS Temperature error**                    [°C] 0.045
  Ledge Max (infinite norm) Iter. Disp.***         [mm] 0.1
  Number of global iterations                      [-]  35
  FEA Heat imbalance                               [W]  2.83
  FEA Heat imbalance                               [%]  2.81E-03
=============================================================
```

** Refers to the maximum absolute computed difference with the bath melting temperature for an individual node at the ledge-liquids interface.*
*** Refers to the root mean square difference computed with the bath melting temperature for all nodes at the ledge-liquids interface.*
**** Refers to the maximum absolute computed iterative displacement for an individual node at the ledge-liquids interface.*

Figure 6. Standardized output example.

3. Modernized Approach Features

The present work follows the recommendations of Arkhipov et al [6] and includes the bath and the metal pad in the electrical problem to obtain a representative current distribution in the metal pad and an accurate anode voltage drop. However, the liquids are assumed to be isothermal at the operating temperature and are not part of the thermal domain. The liquids are split into a fixed part and a moving part that follows the ledge.

The latest generation ANSYS elements are used for the calculations. These elements are compatible with the high-performance computing solvers, including the Distributed Domain sparse Solver (DDS) that was employed to solve the full quarter model. The finite element mesh can be linear or quadratic, which enables a tetrahedral mesh to be used with excellent accuracy for the entire calculation domain with the exception of the ledge and the moving liquids, given that these need to be structured as required by the ledge repositioning logic.

3.1 Ledge Repositioning Logic

During preprocessing, auxiliary matrices and local coordinate systems are built and stored. This data structure is reused for every ledge moving iteration thus considerably reducing the overall time spent accessing the ANSYS database over the course of the global problem solution. The data structure is built in such a way that it can be easily expanded. Several additional controls were implemented to overcome convergence difficulties with a particularly challenging lining design, including:

The introduction of different ledge displacement relaxation factors by ledge zone (sidewall/end wall and lower/upper portions);
The usage of an absolute displacement cut-off during a moving iteration, defined by ledge zone (sidewall/end wall and lower/upper portions).

The moving logic was generalized to handle either linear or quadratic elements as well as an arbitrary number of elements through the ledge thickness. The construction of the auxiliary matrices is based on the connectivity of the finite element mesh instead of the spatial position of the nodes, which makes the routines generic to any geometry with a structured (but not necessarily uniform) ledge mesh. This feature can easily handle dissimilar side and end lining profiles – refer to Figure 7 – as well as arbitrarily shaped ledge profiles.

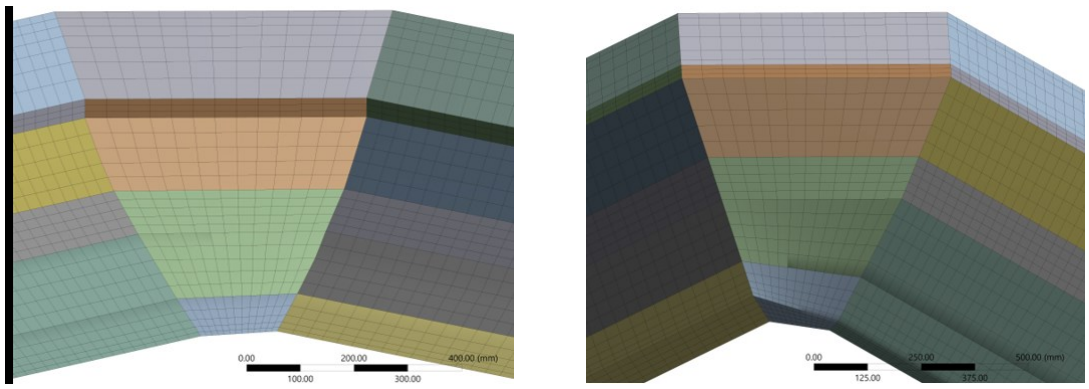

Figure 7. Structured, non-uniform ledge FE mesh originating from dissimilar side and end lining profiles. Left: as seen from the inside of the cell. Right: as seen from the outside of the cell looking up.

As the nodes within the ledge are repositioned to obtain the bath melting temperature at the interface with the liquids, the nodes in the moving liquids are also repositioned to maintain element aspect ratios within appropriate limits in order to obtain an adequate current distribution. An example for a quadratic mesh is shown in Figure 8.

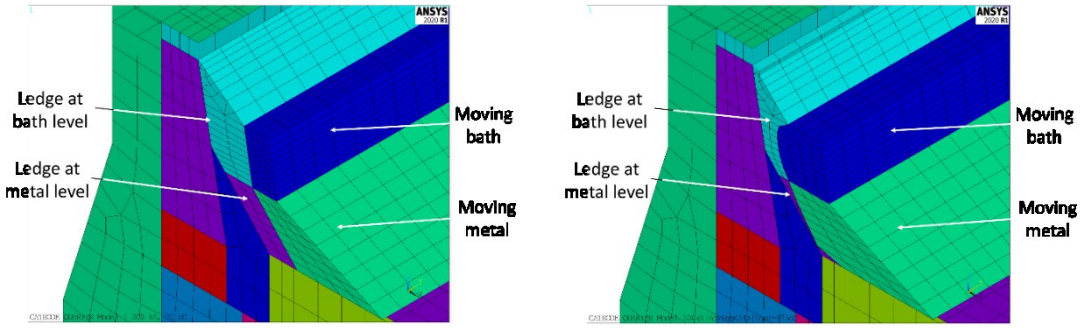

Figure 8. Initial and final 2nd order FE mesh for ledge and moving liquids. Left: initial mesh. Right: converged ledge profile mesh.

The convergence of the ledge profile is based on the infinite norm of the temperature difference with the bath melting temperature and/or on the infinite norm of the iterative ledge displacement.

As previously mentioned, an important aspect of this work is that the ledge, the cathode and the metal pad have independent meshes that are reconnected by contact elements. This allows the ledge to freely move on the cathode surface irrespectively of the cathode topology. The ledge displacement outwards (*i.e.*, towards the center of the cathode panel) is constrained only by the external surface of the moving liquids zone and, inwards (*i.e.*, towards the potshell), by the cell lining geometry.

3.2 Heat Balance Solution

Dupuis's approach [3] is used to converge the heat balance solution. This involves iteratively solving the thermal-electrical problem until the heat imbalance, *i.e.* the difference between the cell internal heat and the total heat losses, is less than the convergence criterion AND the ledge profile has converged. This scheme assumes a fixed bath chemistry. Therefore, for each global iteration, a new thermal-electrical solution must be found, the voltage drops are obtained from the finite element solution, a new cell internal heat is calculated, the cell heat losses are integrated over the control volume and the convergence metrics are computed. If the global problem has met the aforementioned criteria, the solution is done and the postprocessing is performed. Otherwise, a new operating temperature is calculated, the ledge profile is repositioned, heat transfer boundary conditions are updated and a new global TE solution is computed.

The calculation of the cell internal heat is based on the APDL implementation of the steady-state cell voltage and heat balance routines used in the dynamic cell simulators ARC/Dynamic and Dyna/MARC [7].

A generic iterative heat balance convergence scheme was implemented to predict both the superheat and the ledge profile at the same time, which proved to be slow but robust – refer to Figure 9. A standard Newton-Raphson convergence method – typically applicable for well-behaved problems – is also available. Nevertheless, it must be stressed that it showed a tendency to diverge for challenging lining designs, such as the one previously mentioned in section 3.1.

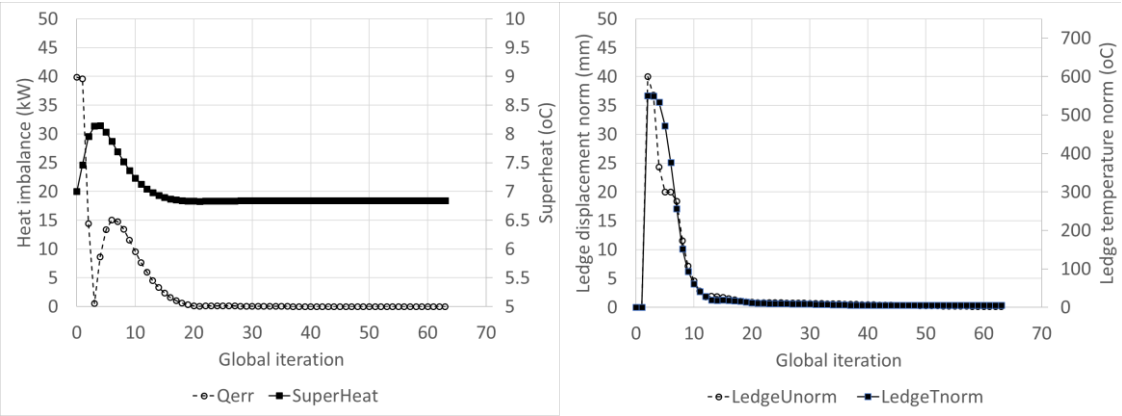

Figure 9. Global heat balance and ledge profile convergence example. Left: superheat and heat imbalance, Right: ledge convergence infinite norms.

3.3 Standardized Output

The detailed heat losses reported in the standard output file are independent of the heat losses calculated for the complete cell used for converging the heat balance. The definition of these

surfaces is entirely up to the User, which is particularly useful when planning a measurement campaign for model validation. The output surfaces can therefore be defined to match what can be measured in practice and refined to the level of details appropriate for the task at hand.

In the standard output file previously shown in Figure 6, the `[Component]` column corresponds to a named selection on which the heat flow is integrated, except for two lines:

`Heat leaving cathodic CV`
: Refers to the heat flow leaving the defined cathodic control volume. This contribution is used in the cell heat balance;

`Joule Heat outside cathodic CV`
: Refers to the Joule heat generated in the elements outside the control volume. This heat input is not considered in the cell heat balance.

In this work, the control volume boundary is at the end of the cathodic flexes and there are no elements outside the cathodic control volume. The anode rod elements located outside of the enclosure, on the other hand, are excluded from the control volume.

4. Model Results with the Standard Ledge Topology

Within the context of this work, the demonstration model previously used by Dupuis (refer, for example, to [2]) was rebuilt in the modernized environment with the standard ledge topology, shown in Figure 8. In this configuration, the ledge toe moves parallel to the cathode surface and, in order to allow for a direct comparison between the two (2) distinct approaches, a linear mesh was used.

The heat balance problem was solved with both platforms using the same material properties, boundary conditions and key simulation parameters – the latter of which shown in Table 1.

Table 1. Comparison case main process parameters.

Parameter	Unit	Value
Cell amperage	[kA]	300.0
Excess (dissolved) [AlF_3]	%	10.825
Dissolved [Al_2O_3]	%	2.5
[CaF_2]		3.0*
[LiF]		0.0
[MgF_2]		0.0
External voltage	mV	200.0
ACD	cm	5.0
Anode cover thickness	cm	16.0

** Even though not representative of most aluminum reduction cell technologies, the reported CaF_2 content was kept as indicated in order to ensure consistency with previously published data.*

The main heat balance and computational results are summarized in Table 2.

Table 2. Comparison case main heat balance results.

Result	Original Dupuis	Hatch Modernized	Unit
Operating temperature	974.72	974.84	ºC
Liquidus temperature	967.99	967.99	ºC
Superheat	6.73	6.84	ºC
Cell internal heat	639.5	642.4	kW
Anode heat losses	236.3	234.4	kW
Cathode heat losses	403.5	408.0	kW
Total cell heat losses	639.8	642.4	kW
Heat imbalance	0.037	0.000	%
Anode voltage drop	334.3	339.3	mV
Cathode voltage drop	287.2	290.4	mV
Ledge infinite temperature norm*	20.8	5.2	ºC
Ledge RMS temperature norm**	0.15	0.013	ºC
Ledge infinite displacement norm***	1.0	0.1	mm

** Refers to the maximum absolute computed difference with the bath melting temperature for an individual node at the ledge-liquids interface.*
*** Refers to the root mean square difference computed with the bath melting temperature for all nodes at the ledge-liquids interface.*
**** Refers to the maximum absolute computed iterative displacement for an individual node at the ledge-liquids interface.*

The converged ledge profiles are compared in Figure 10, with cyan being for the original Dupuis methodology and purple for the modernized version. The profiles are almost identical at the sidewall, but the ledge toe in the modernized version is longer in the corner.

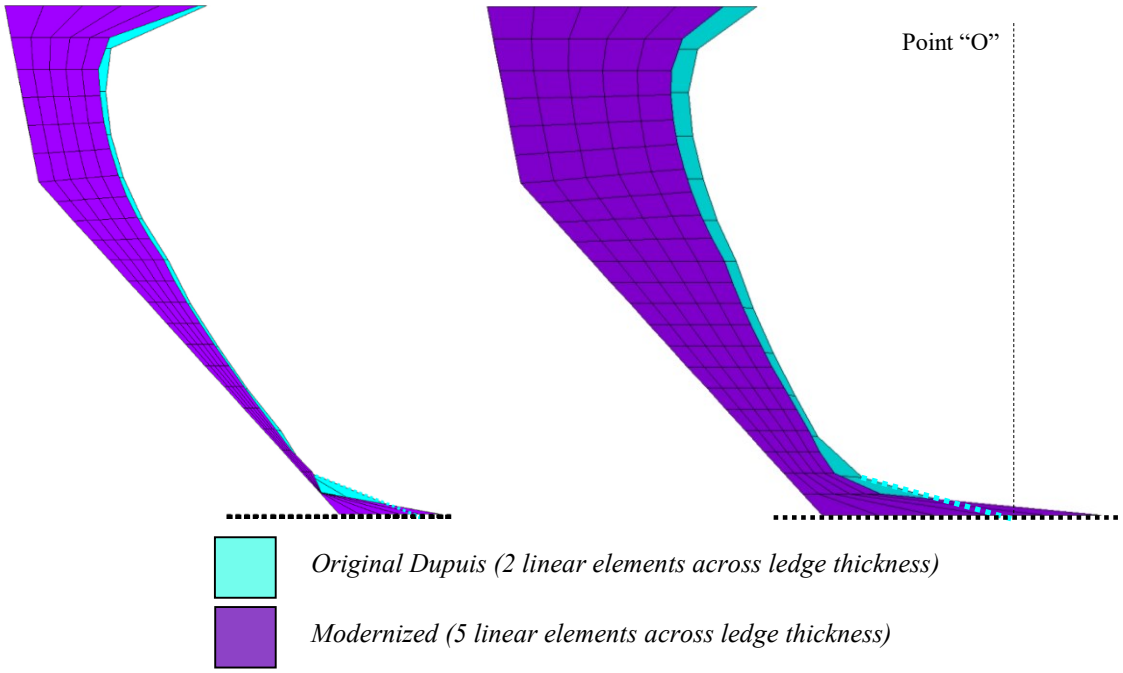

Figure 10. Ledge profiles for the comparison case. Left: sidewall. Right: corner section at 45°.

It was found that the ledge toe is limited in the corner of the original version due to the construction of the cathode block mesh. This is shown in Figure 11 (Left), where the green ledge is constrained by the dotted white line and, as a consequence, the ledge is prevented from moving beyond Point "O" – refer also to Figure 10 (Right). This constraint does not exist in the modernized version shown in Figure 11 (Right) due to the usage of contact-target elements between distinct parts.

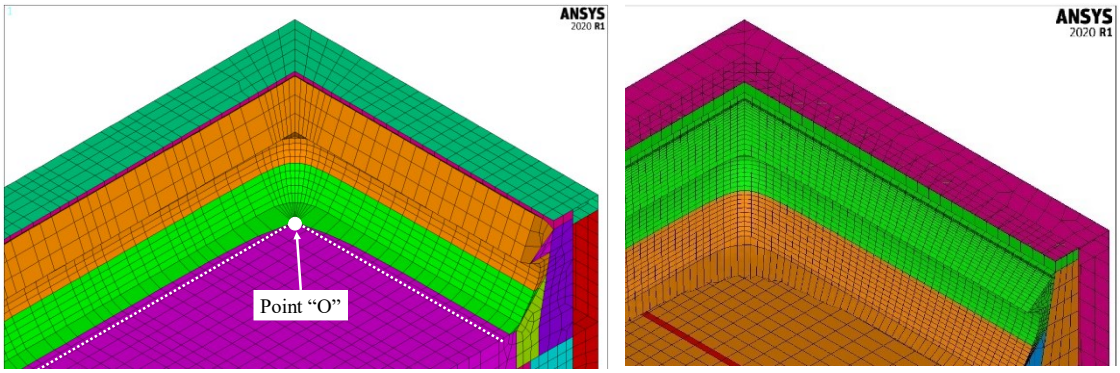

Figure 11. Corner ledge profile meshes for the comparison case. Left: corner ledge movement is limited by the cathode panel-to-ledge mesh connectivity of the original Dupuis model. Right: ledge movement not hindered by the cathode panel mesh of the modernized version.

For the modernized model, the ledge was compared at the same superheat for the linear mesh and a quadratic mesh with only two (2) elements through the thickness. The quadratic mesh was previously shown in Figure 8. The obtained profiles are essentially identical, as shown on Figure 12 (Left) for the sidewall, and on Figure 12 (Right) for a cut through the corner. This built-in capability allows the User to easily perform mesh independence tests to determine the appropriate discretization scheme for the task at hand.

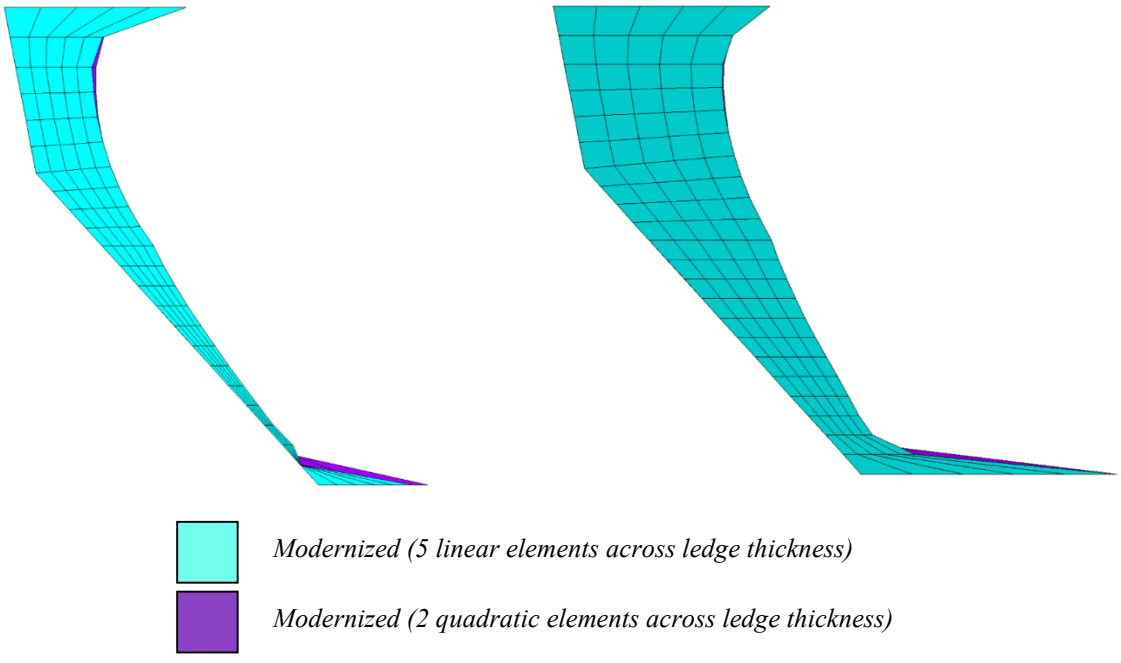

Figure 12. Linear and quadratic ledge profiles for the comparison case. Left: sidewall, Right: corner section at 45°.

For reference, the machine used to solve the modernized models is a 28 core Intel(R) Xeon(R) Gold 6240 CPU @ 2.60 GHz with 128 GB of RAM. The ANSYS/WB database processing was done using 4 cores in Shared Memory Processing mode (SMP) while the solution was performed using the ANSYS sparse Distributed Domain Solver (DDS) with all 28 cores. The maximum memory used was 30 GB of RAM. The elapsed time is detailed in Table 3.

It can be seen that the modernized approach using auxiliary matrices is very efficient since most of the elapsed time is spent computing finite element solutions. In fact, the total elapsed time spent to reposition each and every node of the ledge (including the redefinition of heat transfer boundary conditions) was less than ten (10) seconds per global solution iteration.

Table 3. Modernized full quarter heat balance and ledge convergence computational data.

Task	**Elapsed time (min)**	**Elapsed time (%)**
Process ANSYS/WB database	3.9	2
Solve the global heat balance problem	172.5	98
Elapsed time spent moving ledge	*3.5*	*2*
Elapsed time spent preparing solution	*11.4*	*6*
Elapsed time spent computing solution	*143.8*	*82*
Elapsed time spent postprocessing solution	*1.6*	*1*
Elapsed time spent post-processing model	*12.2*	*7*
Total	176.4	100

Parameter	**Value (-)**
Number of degrees of freedom	534 079
Number of global iterations	64

For the original methodology, which involves building the model from scratch, the elapsed time breakdown in shown in Table 4. Two-thirds of the time is spent in the preprocessor building the model, moving the ledge and updating the boundary conditions. The machine used to solve this model has 2 cores Intel i5-6300U CPU @ 2.40 GHz processors used in Shared Memory Parallel (SMP) processing.

Table 4. Original full quarter heat balance and ledge convergence computational data.

Task	**Elapsed time (min)**	**Elapsed time (%)**
Elapsed time spent pre-processing model	58.9	65
Elapsed time spent solution - preprocessing	0.2	0
Elapsed time spent computing solution	29.7	33
Elapsed time spent solution - postprocessing	0.0	0
Elapsed time spent post-processing model	1.8	2
Total	90.7	100

Parameter	**Value (-)**
Number of degrees of freedom	162 506
Number of global iterations	17

5. Novel Topology

The Authors encountered a challenging industrial lining design that would lead the standard ledge repositioning algorithm to diverge. In this specific design, the ledge tends to grow far in the corner and then melt back at the sidewall and at the end wall. Near the corner, the side ledge and the end ledge move in zones that have very low thermal gradients, such that one node would move

towards the wall and the neighboring node would move towards the cell center, creating "ledge spikes". Unfortunately, the global solution diverges once said spikes were formed.

The cause of the problem is thought to be a combination of cold cathodes, a cold corner and a very insulated end wall. After many trials and refinements to the controls of the allowable ledge displacement (once again, refer to section 3.1), further analysis revealed that it would never be possible to converge the ledge with the standard algorithm since there would always be at least one ledge slice that has two possible solutions for the position of the ledge toe. This is schematically shown in Figure 13.

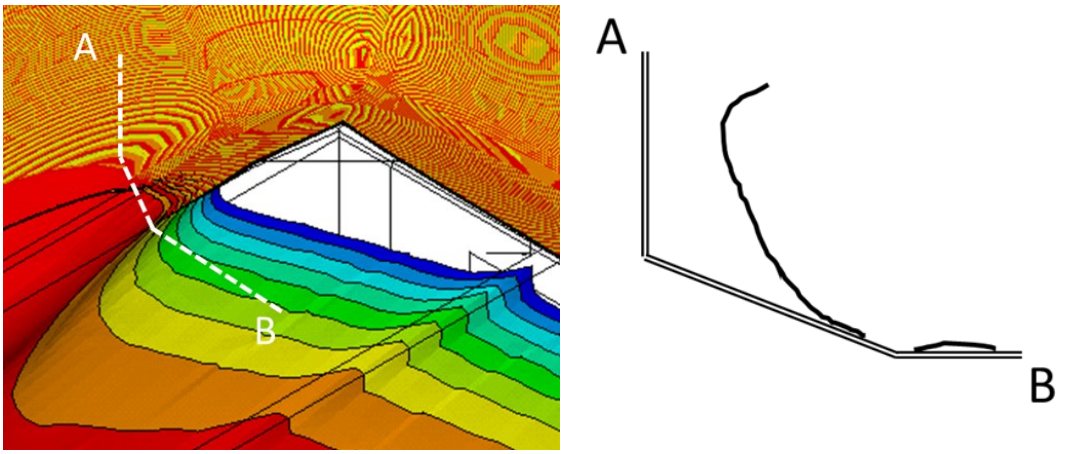

Figure 13. Challenging corner design for the standard ledge repositioning algorithm. Left: temperature isosurfaces in the cell corner, ranging from white (very cold) to blue (cold), to hot (red), Right: ledge profile at slice A-B.

A new ledge repositioning topology was devised in order to allow the ledge to move orthogonally to a set of arbitrary planes, as shown in Figure 14 (Right). The initial solution is performed with the elements on the cathode surface as thermal-only frozen ledge– see Figure 14 (Left). Once the ledge thickness on the cathode surface has been reduced to a prescribed minimum, the elements are switched to liquid metal, therefore being now able to conduct electricity between the remainder of the metal pad and the cathode blocks surface. If the element surface temperature is under the bath melting temperature, the stack of underlying moving elements is turned back to thermal-only ledge properties. The applied thermal boundary conditions are updated at every ledge moving iteration depending on the element status, while the physics of the contact-target element pairs used to connect the different parts is modified accordingly.

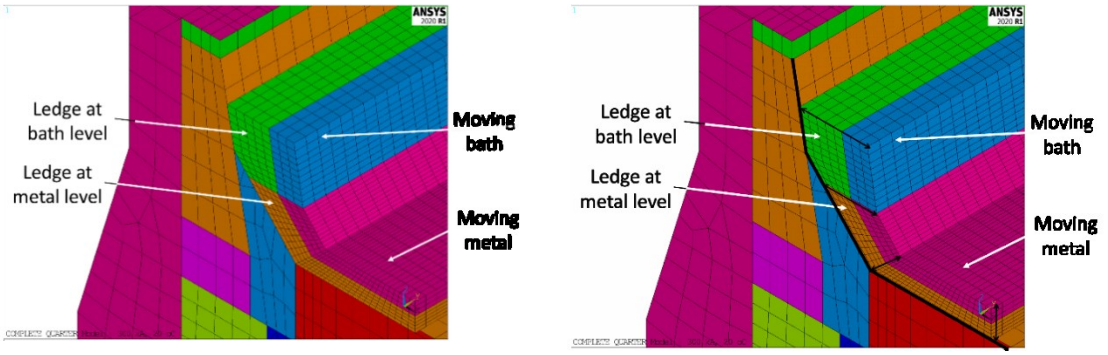

Figure 14. Initial FE mesh and ledge displacement direction for novel ledge topology. Left: initial mesh, Right: ledge displacement direction.

The construction of the ledge repositioning auxiliary matrices is identical to the standard topology since the data acquisition is based on the finite element connectivity of the structured ledge and moving liquids. Additional information was added in the existing data structure to track the specific information required to process the ledge elements on the cathode surface.

The fictitious lining design used for demonstration purposes was modified with adjustments to material properties and boundary conditions to obtain issues similar to those encountered with the real-life stubborn lining design. The modifications made to the original lining design were devised to obtain a cold cathode and a hot end wall. For the sake of simplicity, the problem was solved only for the ledge profile at a constant superheat of 6.5 ºC.

The obtained ledge convergence curves are shown in Figure 15. The standard ledge topology does not converge and oscillates up to the prescribed maximum number of global iterations, while the novel topology converges within 33 iterations.

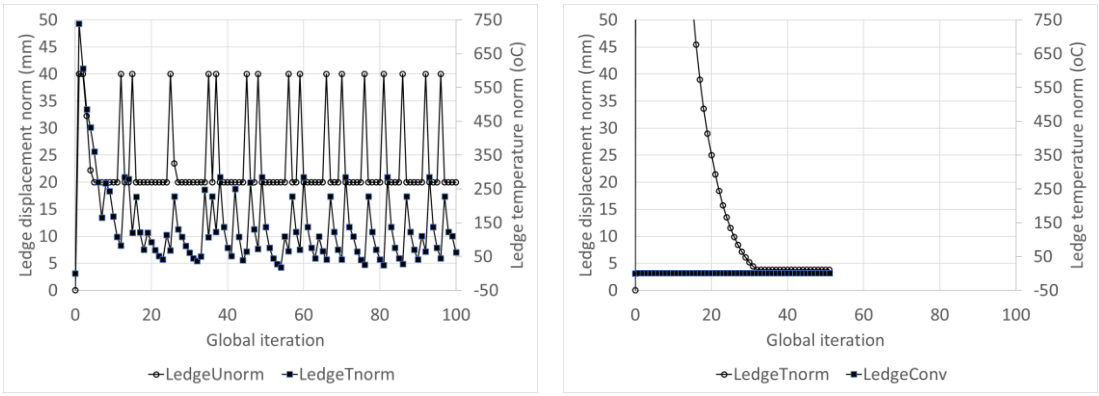

Figure 15. Problematic lining ledge convergence curves. Left: standard topology, Right: novel topology.

The resulting ledge profiles are compared in Figure 16. Even though the whole ledge should have disappeared at the end wall – see Figure 16 (Right) – a "ledge spike" appears for the standard topology in a region of low thermal gradient – Figure 16 (Left). This is due to the fact that the current flow into the center of the block is low as a result of the split bar design with castable in the middle of the slot. Also, the thermal flux extracted by the collector bars is the lowest near the symmetry plane.

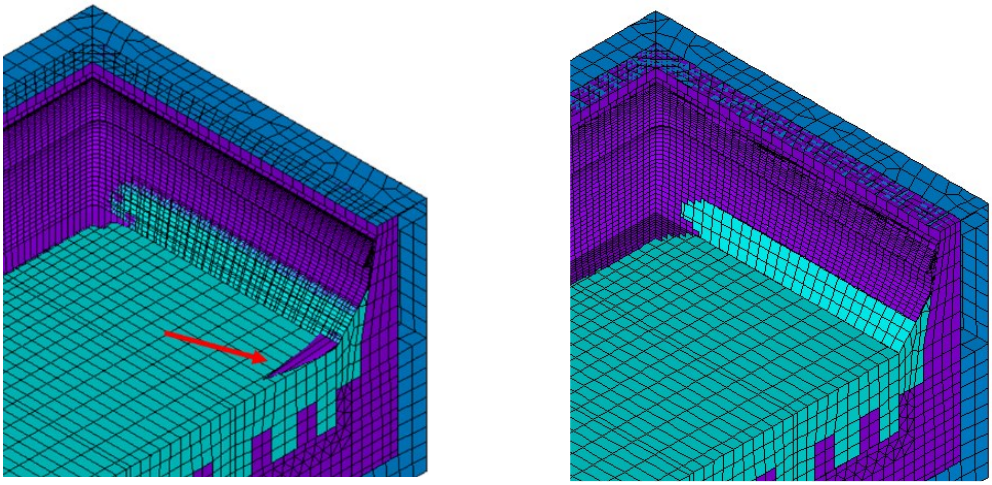

Figure 16. Problematic lining ledge profiles obtained with both standard and novel ledge topologies. Left: non-converged ledge profile for the standard topology, Right: converged ledge profile for the novel topology.

6. Discussion

The novel topology allows solving problems that cannot be converged by the standard approach, particularly when the lining design results in zones of low thermal gradient on the cathode blocks. The ledge toe profile calculated by both methods differs – it is clear from Figure 17 that the standard topology (in purple) produces elongated elements at the ledge toe while the novel topology (in cyan) results in a smooth and thin layer of ledge at the same location.

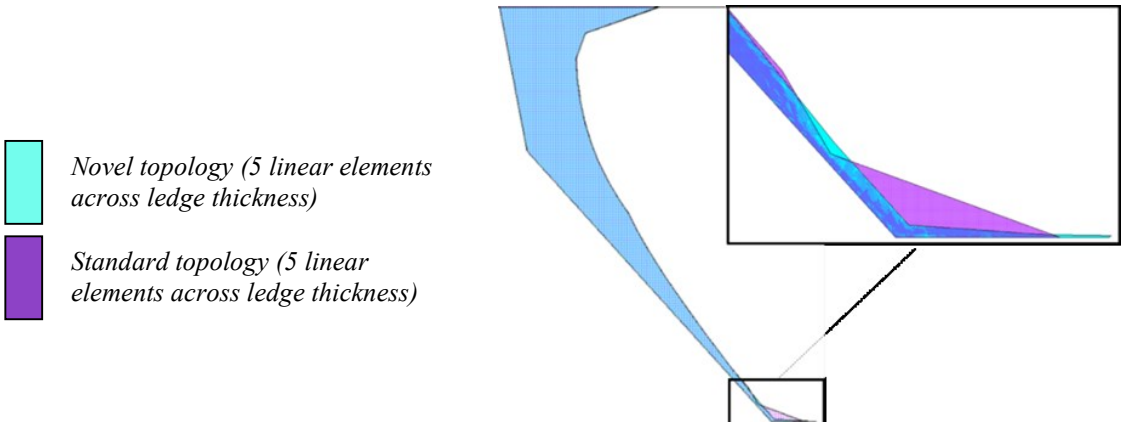

Figure 17. Comparison of ledge profile elevation with standard and novel ledge topologies: ledge toe behavior.

While the ledge profile solution appears better in elevation, one of the drawbacks of the novel topology is the "checkerboard" pattern of the ledge toe introduced by the fixed horizontal discretization of the ledge or, in other words, due to the fact that the ledge is only allowed to move vertically in this region. This is shown in Figure 18 for the standard lining design. Note that this checkerboard pattern effect can be reduced (but not entirely avoided) by refining the FE mesh of the ledge over the cathode panel and by using a different meshing scheme in the corner.

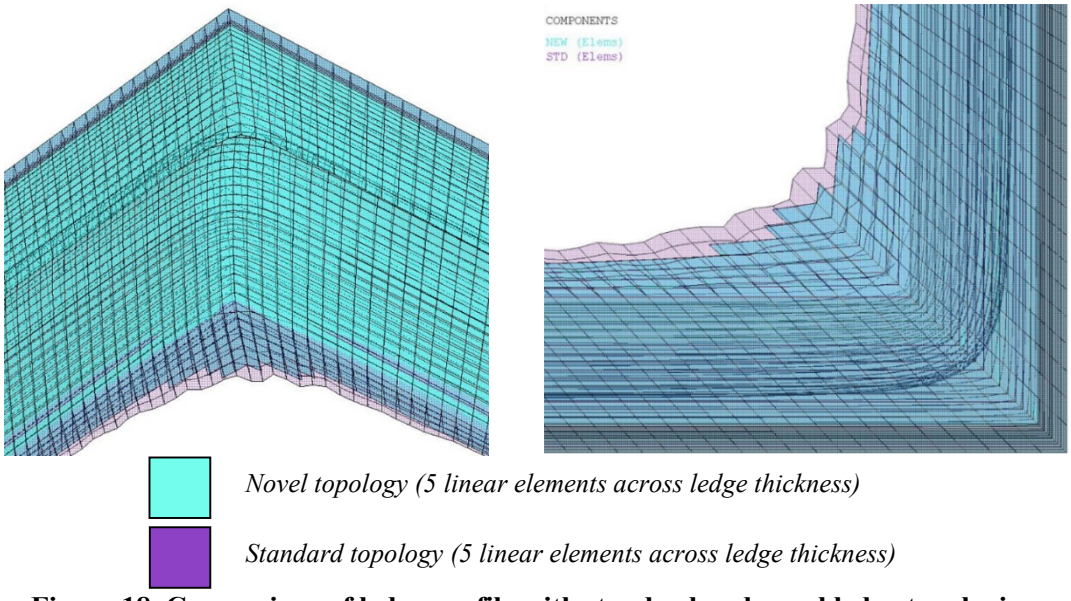

Figure 18. Comparison of ledge profile with standard and novel ledge topologies: checkerboard pattern effect for novel ledge topology. Left: isometric view, Right: plan view.

7. Conclusions

A modernized approach to thermal-electrical finite element modeling of the cell heat balance problem has been developed in the commercial software package ANSYS 2020 R1. The new workflow is based on a combination of an interactive ANSYS/Workbench session, User-edited input text files, and generic APDL scripts running in the background. The main limitations of the original approach were eliminated and the use of the most recent ANSYS element technology enables leveraging the high-performance parallel computing solvers, including the sparse Distributed Domain Solver (DDS).

The modernized model was compared to the original approach for a complete quarter cell heat balance and ledge profile solution and results were found to be very similar. Convergence of the ledge profile was obtained for a linear and a quadratic mesh with (virtually) identical results.

A novel ledge topology was developed based on the displacement of the ledge nodes orthogonally to any arbitrary set of planes. The new topology allows the computation of otherwise impossible to converge problems.

Further work includes experimental validation of the heat balance model and assessment of the ability of the novel ledge topology to accurately predict the position of the ledge toe.

8. Acknowledgements

The authors would like to genuinely express their gratitude to Jack Chapman from Hatch, whose invaluable contributions made this work possible.

9. References

1. Marc Dupuis & Imad Tabsh, Thermo-electric coupled field analysis of aluminium reduction cells using the ANSYS parametric design language, *Proceedings of the ANSYS Fifth International Conference*, Vol 3, 1991, 1780-1792.
2. Marc Dupuis, Thermo-electric design of a 400 kA cell using mathematical models: a tutorial, *Light Metals* 2000, 297-302.
3. Marc Dupuis, Computation of aluminium reduction cell energy balance using ANSYS® finite element models, *Light Metals* 1998, 409-417.
4. Marc Dupuis, Computation of accurate horizontal current density in metal pad using a full quarter cell thermo-electric model, *Proceedings of CIM* 2001, 3-11.
5. Marc Dupuis, How to limit the heat loss of anode stubs and cathode collector bars in order to reduce cell energy consumption, *Light Metals* 2019, 521-531.
6. Alexander Arkhipov et al, Review of thermal and electrical modelling and validation approaches for anode design in aluminium reduction cells, *Proceedings of the 36th Conference and Exhibition of ICSOBA*, Belém, Brazil, Brazil, 29 October - 1 November, 2018, *Travaux* 47, 589-605.
7. Imad Tabsh, Marc Dupuis and Alexandre Gomes, Process simulation of aluminum reduction cells, *Light Metals* 1996, 451-457.